Title
The septin cytoskeleton facilitates membrane retraction during motility and blebbing

Journal
Journal of Cell Biology, 196(1)

ISSN
0021-9525

Authors
Gilden, Julia K
Peck, Sebastian
Chen, Yi-Chun M
et al.

Publication Date
2012-01-09

DOI
10.1083/jcb.201105127

Peer reviewed

The septin cytoskeleton facilitates membrane retraction during motility and blebbing

Julia K. Gilden,[1] Sebastian Peck,[1,2] Yi-Chun M. Chen,[1] and Matthew F. Krummel[1]

[1]Department of Pathology and [2]Biological Imaging Development Center, University of California, San Francisco, San Francisco, CA 94143

Increasing evidence supports a critical role for the septin cytoskeleton at the plasma membrane during physiological processes including motility, formation of dendritic spines or cilia, and phagocytosis. We sought to determine how septins regulate the plasma membrane, focusing on this cytoskeletal element's role during effective amoeboid motility. Surprisingly, septins play a reactive rather than proactive role, as demonstrated during the response to increasing hydrostatic pressure and subsequent regulatory volume decrease. In these settings, septins were required for rapid cortical contraction, and SEPT6-GFP was recruited into filaments and circular patches during global cortical contraction and also specifically during actin filament depletion. Recruitment of septins was also evident during excessive blebbing initiated by blocking membrane trafficking with a dynamin inhibitor, providing further evidence that septins are recruited to facilitate retraction of membranes during dynamic shape change. This function of septins in assembling on an unstable cortex and retracting aberrantly protruding membranes explains the excessive blebbing and protrusion observed in septin-deficient T cells.

Introduction

Cell shape is a result of the interplay between hydrostatic pressure exerting outward force on the plasma membrane, lateral tension of the membrane itself, and contractile forces exerted by the actomyosin cytoskeleton (Sheetz, 2001; Mitchison et al., 2008). Cell shape can largely be explained by varying contributions of these forces. For instance, on the leading edges of crawling cells, protrusion is driven by combinations of densely cross-linked actin and the locally elevated hydrostatic pressure that results from local ion transport and water influx into that region (Stock and Schwab, 2006; Fackler and Grosse, 2008). In contrast, blebs are the result of hydrostatic pressure that causes a segment of plasma membrane to rip away from the cortical actomyosin cytoskeleton, whereas bordering membrane remains firmly anchored by myosin II (Charras et al., 2008). Blebs are actin poor during their expansion phase, and this expansion is limited both by local surface area and by repolymerization of actin on the bleb surface that is associated with retraction (Charras et al., 2006). It has recently been shown that these same forces of positive hydrostatic pressure and contractile actomyosin control cell rounding during mitosis (Stewart et al., 2011).

Septins are a family of GTP-binding proteins that self-assemble into hexameric or octameric quaternary structures and further into large filaments, rings, and gauzes in vitro and in vivo (Kinoshita et al., 2002; Kinoshita, 2003; Rodal et al., 2005). A variety of functions has been described for septins in mammalian cells. Principle among these are contouring of phosphatidylinositol-containing membranes in vitro, templating of actin fibers, stabilization of microtubule tracks, and interaction with exocytic machinery (Kinoshita et al., 1997; Hsu et al., 1998; Surka et al., 2002; Tanaka-Takiguchi et al., 2009; Gilden and Krummel, 2010). Structurally, they appear to be required to maintain cilia and to assist in the completion of phagocytosis (Huang et al., 2008; Hu et al., 2010). The relative importance of each of these roles remains unclear, but knockout animals lacking specific septin subunits exhibit defects in cytokinesis, neuronal development and function, platelet activation, and spermatozoa motility (Kinoshita et al., 1997; Nguyen

S. Peck and Y.-C.M. Chen contributed equally to this paper.

Correspondence to Matthew F. Krummel: matthew.krummel@ucsf.edu

Abbreviations used in this paper: DIC, differential interference contrast; GPI, glycophosphatidylinositol; NPPB, 5-Nitro-2-(3-phenylpropylamino)benzoic acid; RVD, regulatory volume decrease; shRNA, short hairpin RNA.

The Rockefeller University Press $30.00
J. Cell Biol. Vol. 196 No. 1 103–114
www.jcb.org/cgi/doi/10.1083/jcb.201105127

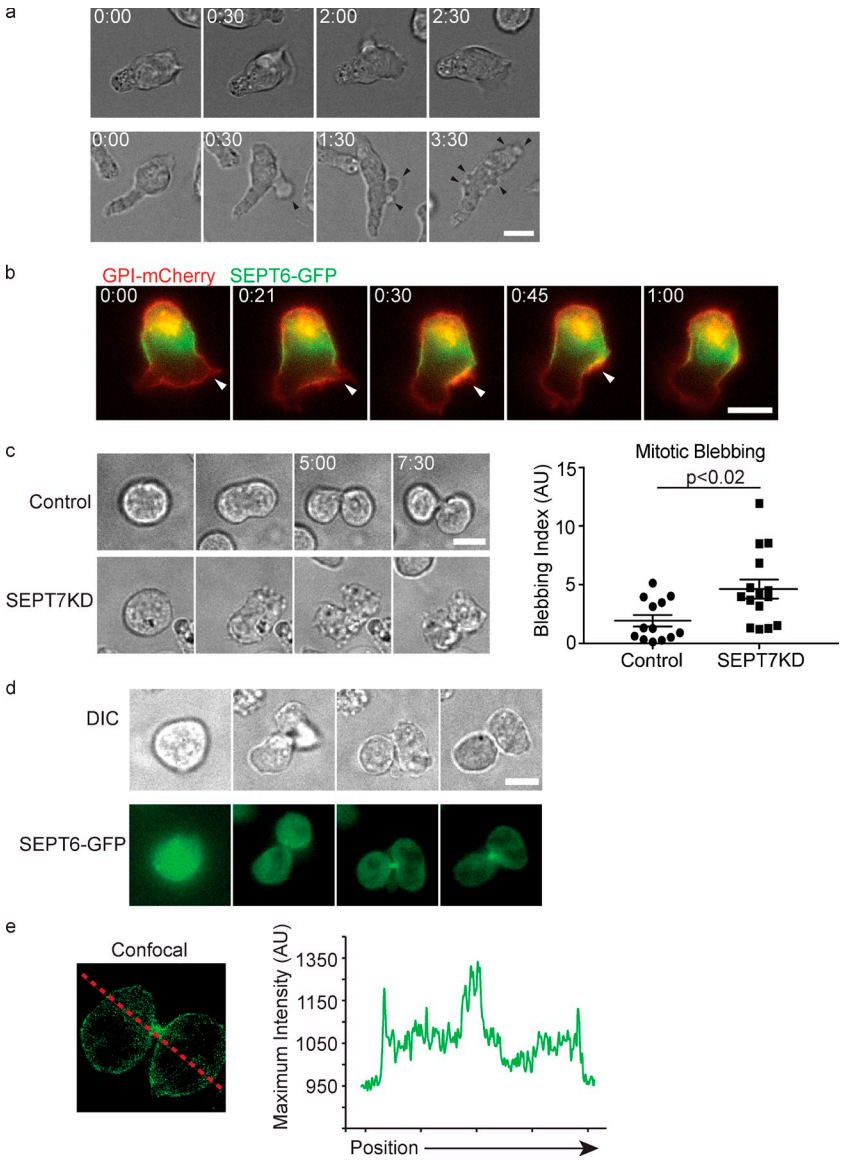

Figure 1. **Septins regulate cortical stability.** (a) D10 T cells crawling on ICAM-1–coated glass display periodic membrane blebs and protrusions (black arrowheads). (b) Fluorescent images of D10 T cells expressing GPI-mCherry and SEPT6-GFP indicate that leading edge protrusions (white arrowheads) retract into the septin collar. $n = 18$. (c) Control and SEPT7KD cells were cell cycle synchronized with nocodazole and then released for imaging. Time-lapse images indicate profound blebbing during cytokinesis among SEPT7KD cells. A blebbing index consisting of the number of blebs divided by the time observed times the cell perimeter was calculated for each cell and indicates significantly elevated blebbing in SEPT7KD cells. Error bars represent SEM. AU, arbitrary unit. (d) Differential interference contrast (DIC) and SEPT6-GFP fluorescence time-lapse images of cells undergoing mitosis as in c, demonstrating accumulations of septin complexes at the midbody late in cytokinesis. (e) A confocal image and linescan demonstrating that a population of SEPT6-GFP remains localized to the cortex during mitosis. The red line indicates the path of the linescan. Bars, 10 µm.

et al., 2000; Dent et al., 2002; Surka et al., 2002; Nagata et al., 2003; Ihara et al., 2005, 2007; Joo et al., 2007).

We have previously shown that extensive septin depletion in amoeboid T cells, via depletion of SEPT7, an essential subunit of septin complexes, leads to a distinctive morphological phenotype that includes excessive blebbing and protrusion along the cell body (Tooley et al., 2009). The observation that septins may play a role in regulating the shape of the cell cortex led us to the current study, in which we sought to understand the interplay between septins and the forces that regulate cell protrusions. To this end, we manipulated the outward hydrostatic pressure experienced by cells and investigated the roles of septins in response to that force. We found that, in aggregate, septins are required for rapid contraction of the cell cortex, in cooperation with the actomyosin cytoskeleton. Septins dramatically assemble at sites of cortical overextension, a class of events that includes both leading edge protrusions before retraction and membrane blebs, where they prove necessary to counteract persistent and extensive blebbing.

Results

Blebbing and protrusion in septin-deficient cells

We have previously shown that cloned T cell lines expressing short hairpin RNAs (shRNAs) against SEPT7 are largely deficient in all septins and have profound morphological defects that include cortical instability (Fig. S1; Tooley et al., 2009). SEPT7KD cells display periodic blebbing as they crawl on coverslips, and a striking feature of these that was not explained in previous work is their prevalence on the forward portions of the cell body but general absence from the uropod (Fig. 1 a). This appears at odds with the observation that the majority of septin aggregates are present along the T cell uropod (Tooley et al., 2009). To better understand how septins function in this process, we expressed a SEPT6-GFP fusion protein in T cells, which, as described for antibody staining against endogenous septins, generally localized to the midzone of the cell in a corsetlike

pattern (Tooley et al., 2009). For comparison with total plasma membrane, SEPT6-GFP was coexpressed with glycophosphatidylinositol (GPI)-linked mCherry, and cells were imaged while crawling on intercellular adhesion molecule–1 (ICAM-1)-coated coverslips. During motility, crawling cells extended protrusions at their leading edges, and these were sparsely populated by septins. Strikingly, when cells changed directions and retracted leading edges, those retracting protrusions frequently (83%; $n = 18$) led to a transient increase in membrane SEPT6-GFP. This accumulation rapidly merged backward into the SEPT6-GFP collar (Fig. 1 b and Video 1). This demonstrated that dynamic enrichment of septins normally occurs at sites of retracting membrane near the leading edge and provided a possible explanation for the extra extensions and blebs that are found in cells lacking this cytoskeleton.

Amoeboid motility is mediated by extensive actomyosin contractile forces originating at the rear of the cell that are thought to generate leading edge protrusions. Because septin deficiency seemed to most prominently affect cortical stability at sites on the membrane that were distant from the major region of myosin contraction in crawling cells, we sought to determine whether septin deficiency also regulated cortical stability at other sites distal to myosin contraction. In cytokinesis, septins colocalize prominently with the contractile actin and myosin at the cleavage furrow. To investigate whether septins might also function distal to the cleavage furrow, control and SEPT7KD D10 T cells were treated with nocodazole for 16 h to synchronize their cell cycles and were imaged during the cytokinesis that followed washout. Though SEPT7 is dispensable for successful mitosis in T cells, an unstable membrane during cell division was indeed readily observed and was notable for occurring mostly distal to the cleavage furrow. Thus, whereas control cells had a mostly smooth plasma membrane during cell division with only a few small blebs occasionally appearing (Fig. 1 c and Video 2), SEPT7KD cells had surfaces studded in tiny blebs, which were also more long lived than those seen on control cells, often persisting from the time of their appearance until the end of the time-lapse, up to 30 min (Fig. 1 c and Video 2). When these blebs were counted, SEPT7KD cells produced, on average, 2.5 times as many blebs per surface area and unit time (blebbing index in Fig. 1 c).

Using SEPT6-GFP–expressing cells, we found GFP primarily concentrated at the cytokinetic furrow during the completion of mitosis (Fig. 1 d), consistent with observations of septins in other mammalian cells and in yeast (Gladfelter et al., 2001; Spiliotis et al., 2005). However, confocal imaging during cytokinesis (Fig. 1 e) emphasized that, whereas SEPT6-GFP is predominantly localized to the cleavage furrow, a septin density is associated with the entire cell cortex, perhaps serving to control mitotic blebs at distal sites. Thus, a line scan through a mitotic cell demonstrates peaks of intensity at each cell border in addition to a large peak at the site of the cytokinetic furrow (Fig. 1 e). Together, these data show that septins are enriched at sites of membrane instability, where they seem to control protrusions and blebs.

Septins are required for cortical retraction in a hydrostatic volume-change assay

These observations suggested the possibility that rather than preventing the onset of protrusions and blebs, septins might be recruited to sites of nascent extension and play a role in resolving those structures after they arise. Either mechanism would give rise to increased numbers of extensions and blebs. To distinguish between those possibilities, we used osmotic volume change as a model for cortical dynamics. Hydrostatic pressure was manipulated by changing the osmolarity of cells' media, and this led to cellular expansion and subsequent contraction. When cells are exposed to hypotonic medium, they respond in two phases: rapid expansion as water flows into the cell followed by a slower regulatory volume decrease (RVD) phase, during which ion transport–dependent processes return the cytosol to its native tonicity and cell volume shrinks (Grinstein et al., 1984). In such an assay, local hydrostatic pressure inside the cell causes the plasma membrane to separate from cortical actomyosin (Charras et al., 2008), effectively generating a cell-wide bleb.

To monitor the progress of this swelling and contraction, cell volume in isotonic media was measured using the forward scatter parameter of a flow cytometer. Cells were then shifted to isotonic media, and their volumes were monitored over time. Three features of cellular swelling and contraction could then be measured: initial volume, maximum volume, and the rate of contraction (or RVD). This experiment is schematized in Fig. 2 (a and b). SEPT7KD and control cells had indistinguishable initial volumes and expanded to the same extent, exhibiting a total change in diameter of 14% for controls and 18% for SEPT7KD (Fig. 2 c). However, the knockdown samples had smaller slopes in the RVD period (0.320 ± 0.021 [SEM] compared with 0.490 ± 0.025 for controls; $P < 0.001$; Fig. 2 d) and took longer to return to their original size (149.7 ± 8.205 vs. 206.0 ± 11.81 s; $P < 0.01$). This indicated that SEPT7KD cells are retarded in their ability to recontract the cortex to its original size and that septins on the whole are required for retraction rather than for preventing initial separation of membrane from the cortical cytoskeleton.

Septin assembly during cortical retraction

To better understand what role septins might be playing during cortical contraction, cells were immobilized on anti-CD44–coated coverslips and stained with antibodies to SEPT7 under isotonic conditions and 10 min after shifting to hypotonic conditions. When cells were immobilized, SEPT7 distribution was less strikingly corsetlike than when cells crawl on ICAM-1 or bare glass (Fig. 3 a). Nonetheless, a clear change in septin distribution was observed when cells were moved to hypotonic media. Under isotonic conditions, 74.6% ($n = 59$) of cells had SEPT7 enriched at the cortex in puncta (Fig. 3 a). After 10 min in hypotonic media, however, only 20% ($n = 75$) of cells had this distribution. The remaining 80% of cells had SEPT7 redistributed into dramatic superstructures. 60% of cells examined had septin fibers, especially at the bottom surface where the cell contacted the coverslip, and 48% of cells had visible ∼1-µm SEPT7 rings on their cortexes (Fig. 3 b). In addition

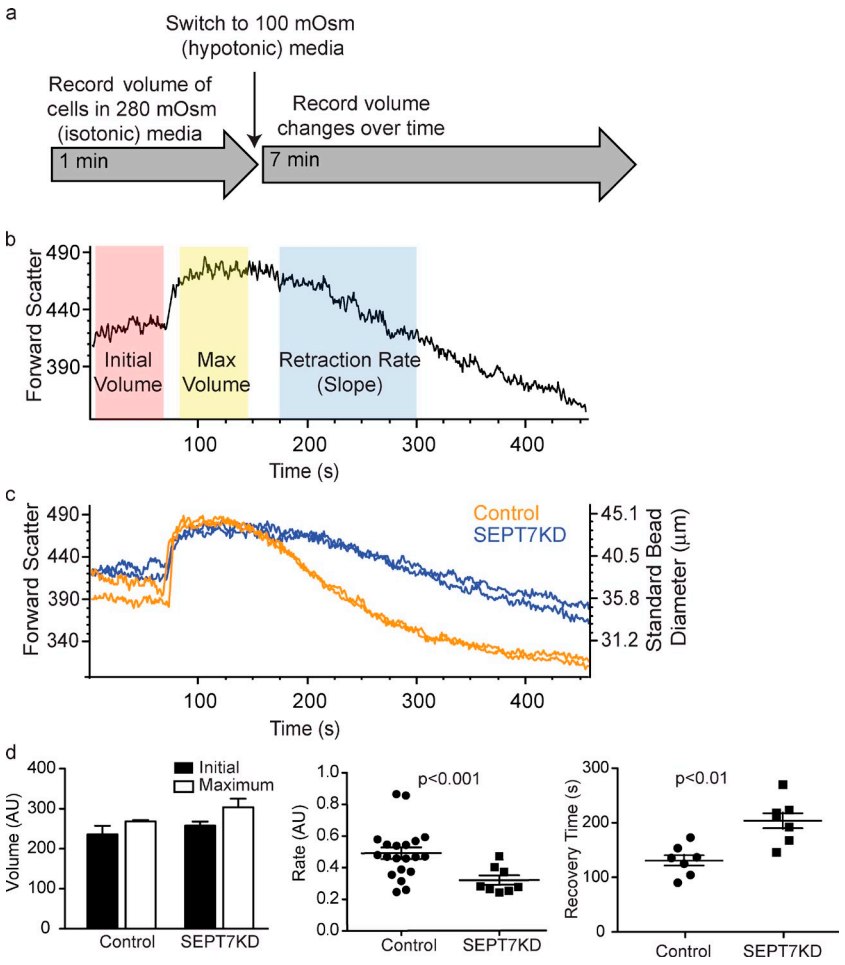

Figure 2. **SEPT7KD cells show slowed retraction in an osmotic swelling assay.** (a) A schematic of a flow cytometry osmotic swelling assay. D10 T cells are suspended in isotonic media, and their volumes are recorded for 1 min. Cells are then switched to 100 mOsm media and returned to the flow cytometer, where changes in their volume are recorded over time. (b) Sample data from osmotic swelling assay indicating time periods in which measurements of initial volume, maximum volume, and retraction (RVD) rate are made. (c) Data from flow cytometry osmotic swelling assay demonstrating normal initial and maximum volumes but slowed RVD in SEPT7KD cells compared with controls. The right axis indicates bead size corresponding with forward scatter values for reference. Two independent samples from each group are shown. (d) Pooled data from four independent experiments showing equivalent initial and maximum volumes for control and SEPT7KD cells but slower RVD rates ($P < 0.001$) and times to return to original volumes ($P < 0.01$) for SEPT7KD samples. Mean and SEM are displayed. AU, arbitrary unit.

to the increase in the frequency of cells with SEPT7 rings, the number of rings per cell (Fig. 3 c) was increased under hypotonic conditions (2.1 ± 1.2 rings per cell for isotonic condition vs. 3.4 ± 2.5 for hypotonic condition; only cells with at least one ring were analyzed).

To observe how septin structures formed in relation to the events of swelling and volume decrease, we monitored the process in real time using SEPT6-GFP–expressing cells. To achieve this, transfected cells were immobilized on anti-CD44–coated coverslips, and after 1 min of imaging, water was added to the imaging chamber to reduce the osmolarity of the media by 2/3. Within 1 min after the change in osmolarity, SEPT6-GFP began to aggregate on the cortex of the cells (Fig. 3 d and Video 3). Over time, these aggregates became pronounced rings, which, when measured, were again on the order of 1 µm in diameter. These expanded in number and ultimately studded the whole surface of the cell and persisted for >30 min (Video 4). These rings were apparent in nearly every cell (Video 5), and the dominance of these circular structures compared with the higher proportions of filaments, seen using anti-SEPT7 antibody staining, may derive from SEPT6 overexpression. When SEPT6-GFP rings were examined more closely in cells coexpressing GPI-mCherry to mark the plasma membrane, dimplelike membrane invaginations could be seen beneath the septin rings (Fig. 3 e and Video 6). This suggested that the structures formed by septins might participate in the confinement or shaping of dynamic membrane.

Septin aggregation is not sufficient to mediate cortical contraction without ion channel function

An important step in the recovery from osmotic expansion is active transport of K^+ and Cl^- ions that return the cytosol to normal osmolarity, and this has been shown to be necessary for RVD (Grinstein et al., 1984). We used charybdotoxin and 5-Nitro-2-(3-phenylpropylamino)benzoic acid (NPPB), inhibitors of Ca^{2+}-gated K^+ channels and of Cl^- channels, respectively, to block ion transport during our flow cytometry volume-change assay. As anticipated, cells treated with the inhibitors had normal volume under isotonic conditions, normal expansion after the shift to hypotonic conditions (Fig. 4 a), and slowed RVD in the presence of both inhibitors (slopes of 0.114 and 0.056 for charybdotoxin and NPPB compared with a slope of 0.323 for untreated control; Fig. 4 b). When SEPT7KD cells were treated with the drugs, neither demonstrated an additive effect on cell shrinkage, though the effect of NPPB was so severe that an additive effect of septin depletion may have been undetectable.

These reagents and their profound block of RVD provided a mechanism to determine whether septins were only recruited as a result of cortical contraction or whether they were recruited

independently and might then function in subsequent steps. When SEPT6-GFP–expressing cells were shifted to hypotonic media in the presence of charybdotoxin or NPPB, they formed SEPT6-GFP rings indistinguishable from those formed by control cells (Fig. 4 c), indicating that septin rings are not sufficient to mediate cell shrinkage if cells cannot recover their normal osmolarity and that formation of septin structures on the plasma membrane does not require cells to effectively shrink.

Septins collaborate with actomyosin to promote cortical retraction and assemble after actin depletion

Rearrangement of the cortical actin cytoskeleton after changes in hydrostatic pressure has been described in several cell types (Cornet et al., 1993; Morán et al., 1996; Pedersen et al., 1999; Carton et al., 2003; Tamma et al., 2007). As interactions of septins with both actin and myosin II have been described, we tested whether the actomyosin cytoskeleton is also required for cell shrinkage after osmotic expansion. None of the inhibitors tested—blebbistatin (a MyoIIA inhibitor), latrunculin B (an actin polymerization inhibitor), or nocodazole (a microtubule inhibitor)—significantly influenced the volume of cells in isotonic media nor their maximum expansion (Fig. 5 a). However, cells treated with latrunculin B shrunk with a rate of 0.289, and those treated with blebbistatin to inhibit MyoII activity shrunk with a rate of 0.347 compared with 0.490 for vehicle-treated cells. In contrast, depolymerization of microtubules with nocodazole had no impact on the rate of volume change (0.453; Fig. 5 b). Thus, both actin and myosin appear to be required to similar extents as septins in this process. Shrinkage of SEPT7KD cells treated with latrunculin B was not additionally impaired, whereas parallel experiments using ion transport inhibitors could have added effects (Fig. 4), suggesting that septins and the actomyosin cytoskeleton may be functioning together to affect cortical contraction (Fig. 5 c).

Immunofluorescence staining for endogenous SEPT7 demonstrated that cells treated with blebbistatin rearranged septin complexes similarly to control cells when hydrostatic pressure was increased, with 64% of cells assembling septin circles or filaments in control cells and 75% assembling these structures in the presence of blebbistatin (Fig. 5, d and e). This suggests that loss of myosin II activity has relatively little effect on septin distribution in either steady-state or swelling responses. In contrast, latrunculin B treatment induced the spontaneous formation of SEPT6-GFP rings even under isotonic conditions, and these rings persisted under hypotonic conditions (Fig. 5 f). These data suggest that septin assembly after osmotic expansion might be triggered by actin depolymerization, a result consistent with a previous study in a fibroblast cell line (Kinoshita et al., 2002). When cells were treated instead with jasplakinolide to stabilize actin filaments, cells rounded up and lost their characteristic septin band at the midzone and instead had SEPT6-GFP distributed diffusely or in small puncta, resembling the distribution seen in untreated rounded cells (Fig. 5 f and Video 7). Importantly, SEPT6-GFP rings were not formed after jasplakinolide treatment, demonstrating that disruption of normal actin dynamics alone was not sufficient for

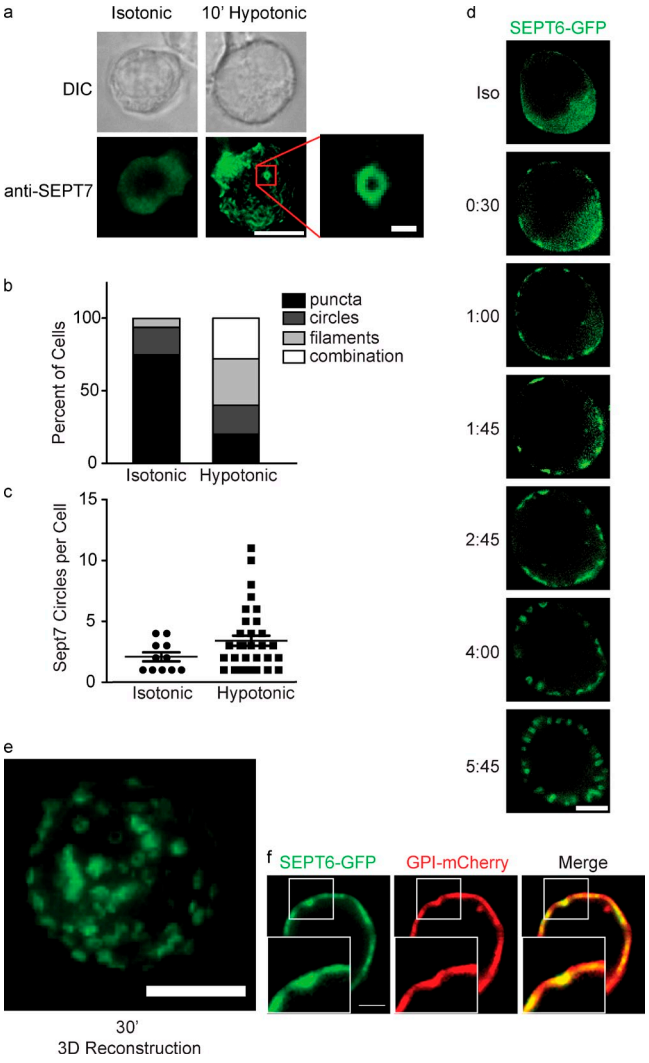

Figure 3. **Septins assemble on the cell cortex during cortical retraction.** (a) DIC and fluorescence images of wild-type D10 cells immobilized on anti-CD44–coated glass and stained for SEPT7 before or after a shift to 100 mOsm hypotonic media. Under isotonic conditions, SEPT7 is enriched at the cortex diffusely or in small puncta. Bar, 10 µm. (inset) Under hypotonic conditions, septins aggregate into filaments and rings. Bar, 1 µm. (b) Quantification of septin distributions observed in a. (c) Though some SEPT7 circles are observed in cells under isotonic conditions, each cell contains a greater number of rings under hypotonic conditions. Error bars represent SEM. (b and c) Representative data from one of two independent experiments performed. (d) Live imaging of SEPT6-GFP–expressing cells shifted to hypotonic media. Within 30 s, SEPT6-GFP begins to aggregate on the cortex and soon assembles into cortical rings that sometimes resemble tubules. Bar, 10 µm. (e) 3D reconstruction of SEPT6-GFP rings 20 minutes after a shift to hypotonic media. Bar, 10 µm. (f) SEPT6-GFP aggregations colocalize with invaginations in the plasma membrane, as indicated by GPI-mCherry fluorescence. Insets show boxed areas in greater detail. Bars, 2 µm.

septin ring formation. In conclusion, septins collaborate with the actomyosin cytoskeleton during cortical retraction. Although MyoII inhibition doesn't affect septin ring formation, ring formation and/or assembly is enhanced by loss of actin integrity through drug treatment or in the course of normal cellular events.

To investigate in more detail the nature of the collaboration between septins and the actomyosin cytoskeleton during

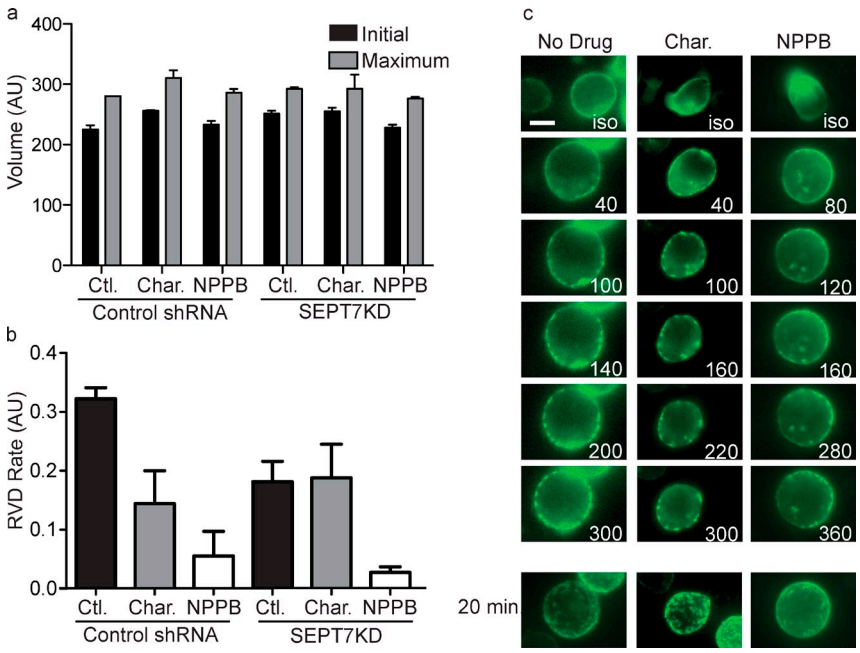

Figure 4. **Septin aggregates are independent of ion transport.** (a and b) Treatment with ion channel inhibitors charybdotoxin (Char.) and NPPB did not influence initial or maximum volume of control (Ctl.) or SEPT7KD cells in the flow cytometry osmotic swelling assay, but both drugs significantly inhibited RVD. Data are pooled from three independent experiments. Error bars represent SD. AU, arbitrary unit. (c) Single-plane time-lapse images of SEPT6-GFP–expressing control cells or cells treated with charybdotoxin or NPPB demonstrate that swelling-induced septin assembly on the cortex can occur in the absence of volume recovery. The bottom row of images taken 20 min after a media change are 3D reconstructions of whole cells. Bar, 10 µm.

cortical retraction, we coexpressed SEPT6-GFP and LifeAct-Ruby in D10 cells and imaged them during RVD using confocal microscopy. Under isotonic conditions, LifeAct-Ruby was homogeneously distributed on the cell cortex. After the shift to hypotonic conditions, however, the cells formed rufflelike actin-rich protrusions (Fig. 5 g and Video 8). Interestingly, these protrusions were septin deficient when they arose, but within 20 s, SEPT6-GFP began to accumulate at their bases, persisting there throughout the retraction of each ruffle. These observations demonstrate a spatial relationship betweens septins and F-actin during RVD and suggest that septins may play a role in regulating retraction through their accumulation at the edges of actin-rich structures.

Septins reshape membrane during cortical contraction

Under many conditions, including swelling, cells respond to cortical stretch initially by smoothing local surface topography such that excess plasma membrane from ruffles and microvilli is recruited into the region under tension (Grinstein et al., 1984). As septins have been implicated in membrane contortion in vitro (Tanaka-Takiguchi et al., 2009) and as we observed topographical changes at the plasma membrane with the assembly of septin rings (Fig. 3 e), we sought to establish whether septins' role in cell shrinkage might be to recontort excess plasma membrane. To investigate this, we took advantage of the side scatter parameter of a flow cytometer, which measures laser light scattered orthogonal to the direction of incident light and correlates with a cell's membrane complexity. When we tracked the side scatter of cells subjected to hypotonic stress, we found that during the hydrostatic expansion phase, there was a precipitous drop in the mean side scatter value followed by a gradual rise over the remaining duration of the experiment, coincident with cortical contraction (Fig. 6 a). When we compared control and SEPT7KD cells, we found that they had similar initial side scatter values, but after the initial drop, SEPT7KD cells recovered more slowly than control cells (slope of 0.029 ± 0.015 for SEPT7KD compared with 0.061 ± 0.014 for controls; Fig. 6, a and b). This indicates that SEPT7KD cells have a defect in recovering membrane complexity concurrent with their slowed shrinkage.

As septins accumulated around actin-rich protrusions and appeared to promote reshaping of excess plasma membrane during RVD, we wanted to test whether they also serve this function in more physiological structures such as blebs. We reasoned that as dynamin activity is required for many endocytic pathways, dynamin blockade would result in excess plasma membrane in need of recapture, possibly by septins. Indeed, when cells were treated with dynasore for 30 min before imaging, they displayed grossly normal morphology, but over a 10-min imaging period, 60% of cells underwent membrane blebbing at the front half of the cell (unpublished data). Interestingly, this blebbing resembled that previously observed in SEPT7KD cells in that it was stochastic and episodic, with cells crawling normally before blebbing began and resuming normal crawling after the blebbing resolved. By treating SEPT6-GFP–expressing cells with dynasore, we were able to use confocal microscopy to directly observe the response of septins to membrane blebs. Before the onset of blebbing, SEPT6-GFP retained its distinctive midzone distribution in the presence of dynasore, and septin circles were not typically observed. This is illustrated in a plot of fluorescence intensities measured around the perimeters of cells, which show two distinctive enrichments of SEPT6-GFP, representing the midzone (Fig. 6 c, top). When cells began to bleb, however, SEPT6-GFP lost its standard midzone distribution and accumulated more evenly around the cortex of dynasore-treated cells, as demonstrated in the generally flat traces in the bottom plot of Fig. 6 c and in Video 9. Notably, this loss of septin polarization is apparent even though cells generally remain polarized while

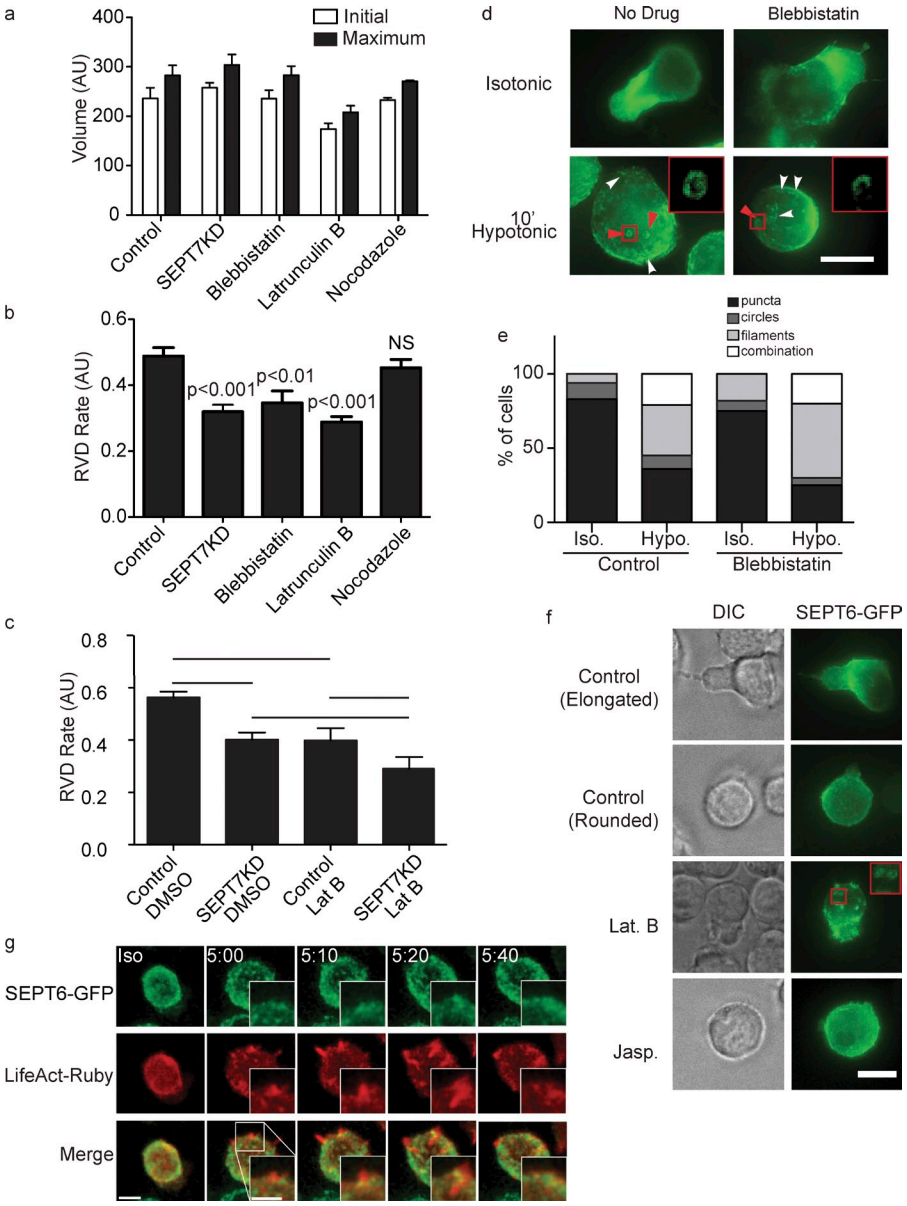

Figure 5. **Interplay between septins and the actomyosin cytoskeleton in cell shrinkage.** (a) Treatment with inhibitors of MyoII (blebbistatin), actin polymerization (latrunculin B), or microtubule polymerization (nocodazole) does not influence initial or maximum cell size in the flow cytometry osmotic swelling assay. AU, arbitrary unit. (b) Cortical retraction in this assay is slowed by blebbistatin or latrunculin but unaffected by nocodazole. (a and b) $n = 7$. (c) There is no additive or synergistic effect on cortical retraction of latrunculin B (Lat B) treatment of SEPT7KD cells. Lines indicate the groups between which statistical posttests were performed after analysis of variance. $n = 5$. (a–c) Error bars represent SD. (d and e) Illustration and quantification of anti-SEPT7 staining of wild-type cells showing that formation of septin filaments (white arrowheads) and rings (red arrowheads) is normal in cells treated with blebbistatin (pooled data from two independent experiments). Insets in d show septin rings in the boxed areas. Hypo, hypotonic; Iso, isotonic. (f) Imaging of SEPT6-GFP–expressing cells demonstrates septin aggregation into rings with latrunculin B treatment under isotonic conditions, whereas no such aggregation was observed with jasplakinolide (Jasp.) treatment. The inset shows latrunculin B–induced septin rings in greater detail. (g) Confocal imaging of cells expressing SEPT6-GFP and LifeAct-Ruby showing actin ruffles with subsequent recruitment of SEPT6-GFP to their bases. Bars, 10 µm.

blebbing. High-resolution confocal imaging of individual blebs in these cells indicated that during initial bleb expansion, the bleb membrane was remarkably deficient in SEPT6-GFP. However, septins accumulated at the fully expanded bleb membrane and remained enriched there during bleb retraction (Fig. 6 d).

Actin has also been shown to polymerize on blebs during their retraction phase (Charras et al., 2006), so we sought to examine how septins and actin interact on these structures. To this end, we used confocal imaging to visualize SEPT6-GFP and LifeAct-Ruby on dynasore-induced blebs. As demonstrated in Fig. 6 e and Video 10, LifeAct-Ruby was recruited to blebs shortly after their appearance, though the structures remained empty of SEPT6-GFP. 10–20 s later, however, SEPT6-GFP was recruited to the retracting bleb, remaining enriched there throughout retraction. This is consistent with our finding that septins were recruited to actin-containing ruffles, apparently participating in their retractile phase (Fig. 5 g). In sum, these data demonstrate recruitment of septins after actin polymerization on unstable dynamic membranes in a variety of settings and suggest a function for septins in providing a platform for membrane reabsorption.

Discussion

Mechanisms of septin-mediated membrane recapture

In this study, we investigated the mechanistic role of the septin cytoskeleton in controlling the T cell cortex. We observed abnormally frequent and persistent membrane blebs during motility and during cell division in septin-deficient cells and found that retracting protrusions in crawling cells usually resolve into the septin-rich midzone of the cell. These findings led us to develop an experimental system in which local blebs were modeled by global hypotonic expansion of the whole cell and bleb retraction was modeled by compensatory RVD. This system

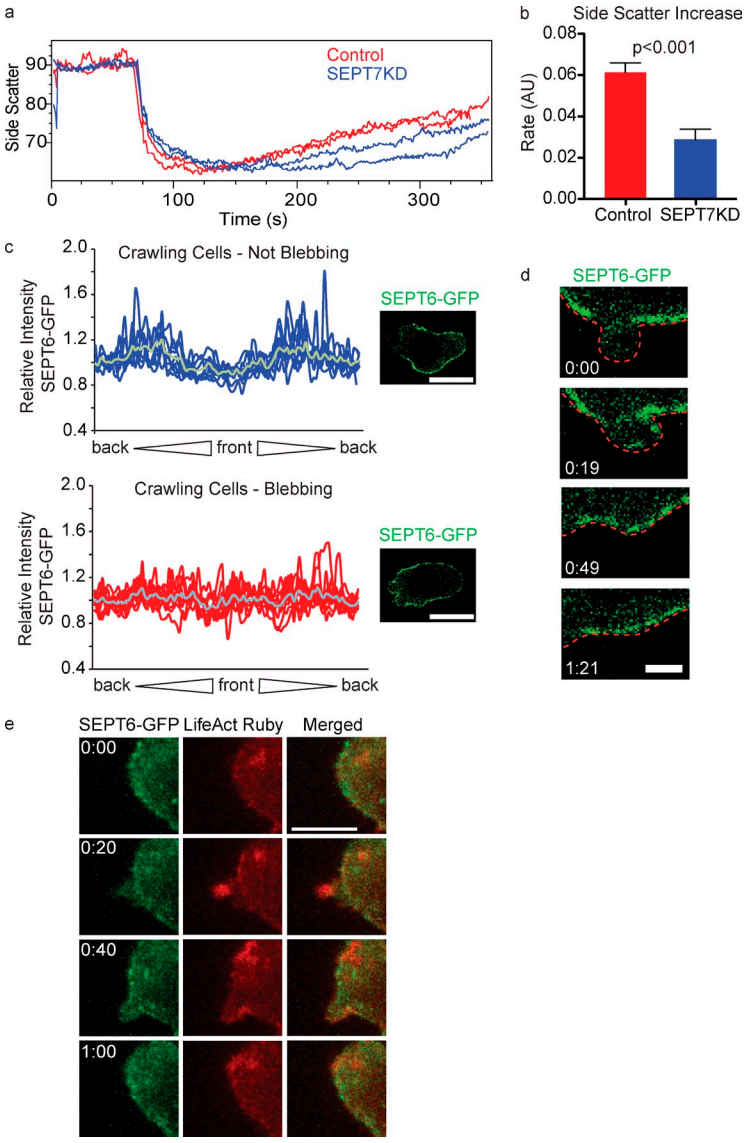

Figure 6. **Septins recapture excess membrane.** (a) Side scatter measurements of control and SEPT7KD D10 cells in the flow cytometry osmotic swelling assay, demonstrating that scattering drops upon the shift to hypotonic media and then gradually returns to isotonic levels. SEPT7KD cells are inhibited in their return to normal side scatter values. The graph shows two samples each of control and SEPT7KD cells. (b) Summary of data from three independent experiments showing a significant decrease in the rate of side scatter recovery in SEPT7KD cells. Error bars represent SD. AU, arbitrary unit. (c) Relative GFP fluorescence along the perimeter of dynasore-treated cells during normal crawling (top) or during blebbing (bottom), accompanied by sample confocal micrographs from which such measurements were taken. Cell perimeters for analysis were generated by manually tracing the outline of the cell in a corresponding DIC image. The gray line in each graph indicates the mean relative intensity at that point. $n = 9$ in each group. Bars, 10 µm. (d) Time-lapse imaging of SEPT6-GFP–expressing cells treated with dynasore demonstrates recruitment of SEPT6-GFP to an individual bleb concurrent with retraction. The red line indicates the outline of the cell. Bar, 2 µm. (e) Time-lapse images of a dynasore-treated cell demonstrating the appearance of LifeAct-Ruby on a bleb followed by population of that bleb with SEPT6-GFP. Bar, 10 µm.

facilitated easy testing of the influence of various molecular pathways on cortical dynamics by using flow cytometry to monitor cell volume. Using this technique, we found that hypotonic expansion is normal in septin-depleted T cells, inconsistent with a role in reinforcing the membrane, but that contraction was significantly slowed. Combined with the finding that protrusions generally retract into a septin-rich region, these data indicate that in T cells, septins play a general role in the retraction of plasma membrane.

Our observation that septins aggregate at sites of membrane invagination and that septins contribute to membrane retraction is consistent with several in vitro studies of the interactions between septins and lipid bilayers. Purified septins in the presence of cell extracts cause tubulation of giant unilamellar vesicles, and formation of those tubules is enhanced by the presence of phosphatidylinositides, especially PIP and PIP_2 in the membrane (Tanaka-Takiguchi et al., 2009). Similarly, polymerization of purified yeast septins can be directly induced by the presence of PIP_2 in lipid bilayers (Bertin et al., 2010). It follows that these lipids may also play a role in septin recruitment in our cortical retraction model. This would be consistent with a study of Ehrlich ascites cells that demonstrated a drop in total cellular PIP_2 during initial hypotonic swelling and increased PIP_2 production during RVD (Nielsen et al., 2007).

Our work did not address whether phosphoinositides indeed recruit septins to the plasma membrane during cortical contraction. In fact, our experiments suggest the possibility that septins could be recruited directly in response to particular actin dynamics or cellular protrusions. We found that during cortical contraction, septins assemble on the cortex in rings similar to those observed during latrunculin B–induced actin depolymerization in our system and others (Kinoshita et al., 2002). A feature of the response to hypotonic conditions in several cell types is the loss of actin stress fibers and subsequent repolymerization of actin in peripheral patches (Carton et al., 2003; Tamma et al., 2007). Similarly, we have observed dynamic flarelike actin structures arising during RVD, with aggregated septins appearing at their bases. This supports the idea that septins are recruited to the cortex coordinately with actin structures. Further work will be required to understand the precise nature

of these structures, how this intersects with septin recruitment by phosphoinositides, and indeed whether that recruitment relies on actin assembly or other cellular components that themselves also dictate actin assembly. Given the results that actin assembly blockade promotes septin ring assembly, it is tempting to speculate that a cellular sensor of depolymerized actin exists and directs both enhanced assembly and septin membrane recruitment for the purposes of membrane control.

Although in vivo evidence of membrane contortion by septins has not yet been shown, observations of septin localization in several concave cortical structures are consistent with our findings. For example, SEPT2 and SEPT11 are recruited to the phagocytic cup in macrophages, concurrent with PIP_2 accumulation, and the presence of septins on this structure is essential for phagocytosis (Huang et al., 2008). Similarly, PIP_2 accumulation at the mammalian cleavage furrow may also play a role in septin recruitment to that site (Field et al., 2005). Further, septins are required for dendritic spine formation by neurons and associate with the plasma membrane at the concave bases of dendritic spines (Tada et al., 2007; Xie et al., 2007).

The physical mechanism by which septins contort the plasma membrane to function in cortical retraction remains to be explored. Of particular interest will be further investigation of the interactions between the septin cytoskeleton and cortical actin in this setting. An important step in bleb retraction is actin polymerization along the inner surface of the bleb and attachment of actin filaments to the plasma membrane by ezrin/radixin/moesin proteins (Charras et al., 2006). We found that septins accumulated on retracting blebs after this actin polymerization. Together with our observation that septins and the actomyosin cytoskeleton function in concert to contract the cortex during RVD, this suggests a model in which septins function together with actin in bleb retraction, perhaps interacting with newly polymerized actin to pull the bleb membrane back to the still intact cortical actomyosin network.

Despite our finding that septins are recruited to sites of dynamic cortical instability, in the steady state, the majority of septins are present in the relatively static midzone of the cell. There are several reasons why this could be the case. First, the midzone and uropod of the cell may be more dynamic than is generally appreciated, and septins assemble there to continuously control separation between the plasma membrane and cortical actin. Alternatively, septins at the midzone may not be stable there but rather may continuously leave the midzone and be replenished as septin-rich retracted membranes (Fig. 1 b) flow back into this region. Either of those possibilities could provide clues to the uropodal elongation observed in SEPT7KD cells, as either would lead to accumulation of excess unretracted membrane in that region in the absence of septins. Finally, we cannot exclude the possibility that septins have several distinct functions in T cells and that their presence at the midzone and role in elongating the uropod are unrelated to the mechanisms we have described here. The population of septins in the midzone may be more stable than the population we have studied here, and this variation could perhaps be a result of the diversity in the subunit composition of septin complexes.

Septin-mediated membrane retraction in motility

The phenotype of septin-deficient T cells is quite distinct from those observed in other septin-deficient cells. Whereas some cell types, such as neurons and spermatozoa, exhibit morphological changes associated with disruption of septins, in no other system has such dramatic cortical instability been observed. This raises the possibility that septin function in amoeboid cells is different from that in other cell types. Because amoeboid cells such as T cells move very rapidly, their cortexes are extremely dynamic, accommodating the near-constant shape change associated with this rapid motility. Amoeboid cells can adopt a variety of motility modes depending on the 3D environment in which they find themselves (Renkawitz and Sixt, 2010). Among these modes is blebbing motility, in which the major leading edge extension is accomplished via polarized blebbing and myosin-driven cytoplasmic flow (Blaser et al., 2006; Langridge and Kay, 2006). Our observation that septins are involved in bleb retraction in T cells suggests that spatial regulation of septins could play a role in restricting blebs to the leading edges of cells exhibiting this kind of motility. Alternatively, septin regulation could be an important component of switching between blebbing motility and other modes.

Understanding whether the composition of septin complexes controls modes of motility may be of particular importance as more is learned about the contributions of septin dysregulation to tumor metastasis. A growing number of studies have found connections between expression of specific septin monomers or splice variants and tumor metastasis, but a mechanism for this relationship remains to be discovered (Osaka et al., 1999; Montagna et al., 2003; Connolly et al., 2011). Overexpression of several SEPT9 isoforms is associated with enhanced motility and invasion in tumor cell lines, and knockdown of Sept9 in metastatic tumor cell lines reduces motility, invasion capacity, and leading edge protrusion (Chacko et al., 2005; Shankar et al., 2010). As tumor cells have been shown to adopt blebbing motility under conditions that are unfavorable to their more common fibroblast-like motility (Friedl and Wolf, 2003; Sahai and Marshall, 2003), it may be informative to investigate whether SEPT9 contributes to metastasis by modulating when and where blebs and protrusions occur or by enforcing particular motility modes.

Conclusion

Together, our findings provide mechanistic insight into earlier observations of the phenotypes of septin-deficient T cells and demonstrate the first in vivo evidence of the in vitro phenomenon of membrane contortion by septin complexes. Our data suggest that interactions with remodeling actin at membranes may be the dominant mechanism by which septins regulate the cortex of amoeboid cells. These observations add an important new molecular player to our understanding of how cellular protrusions are controlled and retracted. This mechanism of cortical control may have implications for the diversity of amoeboid motility modes and may inform our understanding of how septin dysregulation contributes to metastasis.

Materials and methods

Cell lines

The D10.G4 cell line was maintained in RPMI-1640 supplemented with 10% FCS, L-glutamine, penicillin, streptomycin, β-mercaptoethanol, and 10 U/ml human interleukin-2. As D10.G4 cells were used only for studies of motility and not activation, they were not periodically restimulated, as has been previously described (Tooley et al., 2009). Cells were maintained at a density $<10^6$ cells/ml. A subclone of the D10.G4 line was generated by electroporating cells with the SEPT6-GFP plasmid described in the next section, sorting cells using a cell sorter (MoFlo; Dako), and maintaining in the media previously described supplemented with 50 µg/ml Geneticin for selection.

Plasmids and transfections

All transfections were performed by electroporation using Gene Pulser (Bio-Rad Laboratories). shRNA against Sept7 and control shRNA plasmids were used as previously described (Tooley et al., 2009). Cells transfected with knockdown plasmids for *Sept7* were cotransfected with EGFP-N1 (Takara Bio Inc.) as a marker. SEPT6-GFP consists of the mouse *Sept6* sequence with a 22–amino acid linker sequence added by PCR and cloned into EGFP-C1 (Takara Bio Inc.). mCherry-GPI was a gift from G.S. Baron (Rocky Mountain Laboratories, National Institute of Allergy and Infectious Diseases, Hamilton, MT; Speare et al., 2010). LifeAct-Ruby consists of 17 amino acids from *Saccharomyces cerevisiae* Abp140 (Riedl et al., 2008) subcloned into pCMV-RFP-Ruby-N1 vector (Takara Bio Inc.) via EcoRI–BamHI sites.

Immunofluorescence

For observations of crawling cells, cells were allowed to adhere to poly-L-lysine or 0.2 µg/ml ICAM-1–coated coverslips for 30 min before fixation. For volume-change experiments, chambered coverslips (Thermo Fisher Scientific) were coated with 0.5 µg/ml anti-CD44 antibody (clone IM7) for 60 min and then washed three times. Next, cells were suspended in 150 µl of serum-deficient RPMI-1640 and allowed to adhere to coated coverslips for 30 min. 300 µl of either 37°C deionized water or 37°C RPMI-1640 was added to each chamber (for hypotonic and isotonic conditions, respectively). After these preparations, warmed 16% PFA (Electron Microscopy Sciences) was added to each chamber for fixation at a final concentration of 4% for 10 min. After thorough washing with PBS, fixed cells were blocked with 2% donkey serum and 2% FCS and permeabilized with 0.2% saponin (Sigma-Aldrich) in PBS for 30 min. Cells were incubated with rabbit α-SEPT7 antibody (IBL-America, Inc.) for 120 min in permeabilization buffer, washed, and then stained with secondary antibodies (Jackson ImmunoResearch Laboratories, Inc.) in permeabilization buffer for 60 min and washed again. Samples were imaged immediately or stored at 4°C overnight for subsequent imaging.

Microscopy

Widefield images were acquired on a modified microscope (Axiovert 200M; Carl Zeiss) with a Plan-Neofluar 63× objective (Carl Zeiss). The microscope was fitted with dual excitation and emission filter wheels and a camera (CoolSNAP HQ; Roper Scientific). Image acquisition was performed using MetaMorph imaging software (Molecular Devices). For motility and mitosis imaging, 0.25% low–melting point agarose was included in the media to minimize drift. Time-lapse images were acquired every 30 s for mitosis and hypotonic stress experiments and every 1 or 2.5 s for motility experiments. Live cells were maintained at 37°C during imaging, and fixed samples were imaged at room temperature. For confocal imaging, cells were placed onto Lab-Tek II 8 chamber dishes (Thermo Fisher Scientific) with no. 1.5 coverslip bottoms. Spinning-disk confocal images were acquired using a microscope (Axiovert 200M) with a 63×/1.4 NA oil objective, electron-multiplying charge-coupled device camera (iXon 887; Andor Technology), ProScan III stage (Prior Scientific), and a spinning disk (CSU10; Yokogawa Electric Corporation) with 488- and 561-nm laser lines modulated by an acousto-optical tunable filter (NEOS Technologies) assembled by Solamere Technology Group. Cells were kept at 37°C using an objective and sample heater (Carl Zeiss). The microscope was controlled by MetaMorph software.

Inhibitors

Nocodazole (Sigma-Aldrich) was used at 5 µM for flow cytometry experiments and 13 µM for cell cycle synchronization. Latrunculin B (Sigma-Aldrich) was used at 10 µM. Blebbistatin (racemic) was used at 100 µM. Jasplakinolide was used at 100 nM. Dynasore (Sigma-Aldrich) was used at 80 µM. Charybdotoxin (EMD) was used at 25 nM, and NPPB (EMD) was used at 100 µM. Nocodazole, taxol, latrunculin B, blebbistatin, jasplakinolide, and dynasore stock solutions were in DMSO. Stock solutions of charybdotoxin and NPPB were in water.

Flow cytometry volume-change assay

Cells were suspended in serum-free RPMI-1640 at a concentration of 2e6/ml containing 10 nM SYTOX red stain (Invitrogen) for dead cell exclusion and incubated at 37°C with or without inhibitors at the concentrations indicated for at least 60 min before the assay. To monitor the response to osmotic stress, forward scatter values were recorded over time, and after 1 min of recording, cells were transferred to a hypotonic solution of 100 mOsm sucrose, which contained SYTOX red and inhibitors, as necessary. Samples were kept warm with a water jacket for the length of the 6-min time course. For analysis, no forward or side scatter gates were used. Rather, gating was on SYTOX red–negative and, when necessary, GFP-positive cells. Slopes were computed during the linear phase of contraction between 150 and 300 s from the start of the experiment. Approximate cell size was calculated by using 4.5–45-µm microspheres (Polysciences, Inc.) to create a standard curve and fitting forward scatter measurements of cells to this curve (Fig. S2). All experiments were performed on a FACSCalibur flow cytometer (BD).

Cell cycle synchronization

D10 cells were incubated with 13 µM nocodazole for 16–20 h and were then washed in 15 ml of media four times to remove the drug. They were then resuspended in a small volume and incubated at 37°C in chambered coverslips for 30 min before imaging.

Cell sorting

Cell sorting was performed on a cell sorter (MoFlow) or special order research products (FACSAria II; BD) using 70-µm nozzles.

Analysis and statistics

All flow cytometry analysis was performed in FlowJo (Tree Star), and the FlowJo kinetics platform was used for osmotic volume-change measurements. Images were analyzed in MetaMorph (Molecular Devices) or Imaris (Bitplane) software depending on the type of analysis. MetaMorph was used for 3D reconstructions. The mitotic blebbing index consists of the number of blebs observed divided by the product of the time followed (in seconds) and the circumference of the cell (in micrometers). All statistical analyses were performed in Prism software (GraphPad Software), and individual tests are named in the legends.

Online supplemental material

Fig. S1 shows protein levels of a panel of septins after SEPT7 knockdown. Fig. S2 shows the standard curve used for calibrating cell size in the flow cytometry volume-change assay. Video 1 shows the location of membrane protrusions relative to SEPT6-GFP in a crawling cell. Video 2 demonstrates cortical morphology during mitosis of control and SEPT7KD cells, sequentially. Video 3 shows high-resolution time-lapse images of the formation of septin rings during RVD. Video 4 shows a 3D reconstruction of cells with septin rings. Video 5 shows septin rings appearing during RVD in a field of cells. Video 6 shows invaginations in the plasma membrane during RVD. Video 7 shows SEPT6-GFP distribution in cells treated with jasplakinolide. Video 8 shows septin accumulation at the base of actin-containing protrusions during RVD. Video 9 shows recruitment of SEPT6-GFP to blebs in a crawling dynasore-treated cell. Video 10 shows recruitment of LifeAct-Ruby to a bleb preceding SEPT6-GFP recruitment. Online supplemental material is available at http://www.jcb.org/cgi/content/full/jcb.201105127/DC1.

We thank Jessica Wong for assistance with microscopy and Shuwei Jang and Vinh Nguyen for assistance with cell sorting. We also wish to thank Steve Rosen, Torsten Wittmann, Rachel Friedman, and members of the Krummel laboratory for insightful discussion of this project and Audrey Gerard for critical reading of the manuscript.

This work was supported by the National Science Foundation Graduate Research Fellowship Program (to J.K. Gilden), the Leukemia and Lymphoma Foundation (to M.F. Krummel), and the National Institutes of Health (R01AI52116 to M.F. Krummel).

Submitted: 24 May 2011
Accepted: 30 November 2011

References

Bertin, A., M.A. McMurray, L. Thai, G. Garcia III, V. Votin, P. Grob, T. Allyn, J. Thorner, and E. Nogales. 2010. Phosphatidylinositol-4, 5-bisphosphate promotes budding yeast septin filament assembly and organization. *J. Mol. Biol.* 404:711–731. http://dx.doi.org/10.1016/j.jmb.2010.10.002

Blaser, H., M. Reichman-Fried, I. Castanon, K. Dumstrei, F.L. Marlow, K. Kawakami, L. Solnica-Krezel, C.-P. Heisenberg, and E. Raz. 2006. Migration of zebrafish primordial germ cells: A role for myosin contraction and cytoplasmic flow. *Dev. Cell*. 11:613–627. http://dx.doi.org/10.1016/j.devcel.2006.09.023

Carton, I., D. Hermans, and J. Eggermont. 2003. Hypotonicity induces membrane protrusions and actin remodeling via activation of small GTPases Rac and Cdc42 in Rat-1 fibroblasts. *Am. J. Physiol. Cell Physiol.* 285:C935–C944.

Chacko, A.D., P.L. Hyland, S.S. McDade, P.W. Hamilton, S.H. Russell, and P.A. Hall. 2005. SEPT9_v4 expression induces morphological change, increased motility and disturbed polarity. *J. Pathol.* 206:458–465. http://dx.doi.org/10.1002/path.1794

Charras, G.T., C.-K. Hu, M. Coughlin, and T.J. Mitchison. 2006. Reassembly of contractile actin cortex in cell blebs. *J. Cell Biol.* 175:477–490. http://dx.doi.org/10.1083/jcb.200602085

Charras, G.T., M. Coughlin, T.J. Mitchison, and L. Mahadevan. 2008. Life and times of a cellular bleb. *Biophys. J.* 94:1836–1853. http://dx.doi.org/10.1529/biophysj.107.113605

Connolly, D., Z. Yang, M. Castaldi, N. Simmons, M.H. Oktay, S. Coniglio, M.J. Fazzari, P. Verdier-Pinard, and C. Montagna. 2011. Septin 9 isoform expression, localization and epigenetic changes during human and mouse breast cancer progression. *Breast Cancer Res.* 13:R76. http://dx.doi.org/10.1186/bcr2924

Cornet, M., I.H. Lambert, and E.K. Hoffmann. 1993. Relation between cytoskeleton, hypo-osmotic treatment and volume regulation in Ehrlich ascites tumor cells. *J. Membr. Biol.* 131:55–66. http://dx.doi.org/10.1007/BF02258534

Dent, J., K. Kato, X.-R. Peng, C. Martinez, M. Cattaneo, C. Poujol, P. Nurden, A. Nurden, W.S. Trimble, and J. Ware. 2002. A prototypic platelet septin and its participation in secretion. *Proc. Natl. Acad. Sci. USA*. 99:3064–3069. http://dx.doi.org/10.1073/pnas.052715199

Fackler, O.T., and R. Grosse. 2008. Cell motility through plasma membrane blebbing. *J. Cell Biol.* 181:879–884. http://dx.doi.org/10.1083/jcb.200802081

Field, S.J., N. Madson, M.L. Kerr, K.A.A. Galbraith, C.E. Kennedy, M. Tahiliani, A. Wilkins, and L.C. Cantley. 2005. PtdIns(4,5)P2 functions at the cleavage furrow during cytokinesis. *Curr. Biol.* 15:1407–1412. http://dx.doi.org/10.1016/j.cub.2005.06.059

Friedl, P., and K. Wolf. 2003. Proteolytic and non-proteolytic migration of tumour cells and leucocytes. *Biochem. Soc. Symp.* 70:277–285.

Gilden, J., and M.F. Krummel. 2010. Control of cortical rigidity by the cytoskeleton: Emerging roles for septins. *Cytoskeleton (Hoboken)*. 67:477–486.

Gladfelter, A.S., J.R. Pringle, and D.J. Lew. 2001. The septin cortex at the yeast mother-bud neck. *Curr. Opin. Microbiol.* 4:681–689. http://dx.doi.org/10.1016/S1369-5274(01)00269-7

Grinstein, S., A. Rothstein, B. Sarkadi, and E.W. Gelfand. 1984. Responses of lymphocytes to anisotonic media: Volume-regulating behavior. *Am. J. Physiol.* 246:C204–C215.

Hsu, S.C., C.D. Hazuka, R. Roth, D.L. Foletti, J. Heuser, and R.H. Scheller. 1998. Subunit composition, protein interactions, and structures of the mammalian brain sec6/8 complex and septin filaments. *Neuron*. 20:1111–1122. http://dx.doi.org/10.1016/S0896-6273(00)80493-6

Hu, Q., L. Milenkovic, H. Jin, M.P. Scott, M.V. Nachury, E.T. Spiliotis, and W.J. Nelson. 2010. A septin diffusion barrier at the base of the primary cilium maintains ciliary membrane protein distribution. *Science*. 329:436–439. http://dx.doi.org/10.1126/science.1191054

Huang, Y.-W., M. Yan, R.F. Collins, J.E. Diciccio, S. Grinstein, and W.S. Trimble. 2008. Mammalian septins are required for phagosome formation. *Mol. Biol. Cell*. 19:1717–1726. http://dx.doi.org/10.1091/mbc.E07-07-0641

Ihara, M., A. Kinoshita, S. Yamada, H. Tanaka, A. Tanigaki, A. Kitano, M. Goto, K. Okubo, H. Nishiyama, O. Ogawa, et al. 2005. Cortical organization by the septin cytoskeleton is essential for structural and mechanical integrity of mammalian spermatozoa. *Dev. Cell*. 8:343–352. http://dx.doi.org/10.1016/j.devcel.2004.12.005

Ihara, M., N. Yamasaki, A. Hagiwara, A. Tanigaki, A. Kitano, R. Hikawa, H. Tomimoto, M. Noda, M. Takanashi, H. Mori, et al. 2007. Sept4, a component of presynaptic scaffold and Lewy bodies, is required for the suppression of alpha-synuclein neurotoxicity. *Neuron*. 53:519–533. http://dx.doi.org/10.1016/j.neuron.2007.01.019

Joo, E., M.C. Surka, and W.S. Trimble. 2007. Mammalian SEPT2 is required for scaffolding nonmuscle myosin II and its kinases. *Dev. Cell*. 13:677–690. http://dx.doi.org/10.1016/j.devcel.2007.09.001

Kinoshita, M. 2003. Assembly of mammalian septins. *J. Biochem.* 134:491–496. http://dx.doi.org/10.1093/jb/mvg182

Kinoshita, M., S. Kumar, A. Mizoguchi, C. Ide, A. Kinoshita, T. Haraguchi, Y. Hiraoka, and M. Noda. 1997. Nedd5, a mammalian septin, is a novel cytoskeletal component interacting with actin-based structures. *Genes Dev.* 11:1535–1547. http://dx.doi.org/10.1101/gad.11.12.1535

Kinoshita, M., C.M. Field, M.L. Coughlin, A.F. Straight, and T.J. Mitchison. 2002. Self- and actin-templated assembly of Mammalian septins. *Dev. Cell*. 3:791–802. http://dx.doi.org/10.1016/S1534-5807(02)00366-0

Langridge, P.D., and R.R. Kay. 2006. Blebbing of *Dictyostelium* cells in response to chemoattractant. *Exp. Cell Res.* 312:2009–2017. http://dx.doi.org/10.1016/j.yexcr.2006.03.007

Mitchison, T.J., G.T. Charras, and L. Mahadevan. 2008. Implications of a poroelastic cytoplasm for the dynamics of animal cell shape. *Semin. Cell Dev. Biol.* 19:215–223. http://dx.doi.org/10.1016/j.semcdb.2008.01.008

Montagna, C., M.-S. Lyu, K. Hunter, L. Lukes, W. Lowther, T. Reppert, B. Hissong, Z. Weaver, and T. Ried. 2003. The Septin 9 (MSF) gene is amplified and overexpressed in mouse mammary gland adenocarcinomas and human breast cancer cell lines. *Cancer Res.* 63:2179–2187.

Morán, J., M. Sabanero, I. Meza, and H. Pasantes-Morales. 1996. Changes of actin cytoskeleton during swelling and regulatory volume decrease in cultured astrocytes. *Am. J. Physiol.* 271:C1901–C1907.

Nagata, K.-I., A. Kawajiri, S. Matsui, M. Takagishi, T. Shiromizu, N. Saitoh, I. Izawa, T. Kiyono, T.J. Itoh, H. Hotani, and M. Inagaki. 2003. Filament formation of MSF-A, a mammalian septin, in human mammary epithelial cells depends on interactions with microtubules. *J. Biol. Chem.* 278:18538–18543. http://dx.doi.org/10.1074/jbc.M205246200

Nguyen, T.Q., H. Sawa, H. Okano, and J.G. White. 2000. The *C. elegans* septin genes, unc-59 and unc-61, are required for normal postembryonic cytokineses and morphogenesis but have no essential function in embryogenesis. *J. Cell Sci.* 113:3825–3837.

Nielsen, D.K., A.K. Jensen, H. Harbak, S.C. Christensen, and L.O. Simonsen. 2007. Cell content of phosphatidylinositol (4,5)bisphosphate in Ehrlich mouse ascites tumour cells in response to cell volume perturbations in anisotonic and in isosmotic media. *J. Physiol.* 582:1027–1036. http://dx.doi.org/10.1113/jphysiol.2007.132308

Osaka, M., J.D. Rowley, and N.J. Zeleznik-Le. 1999. MSF (MLL septin-like fusion), a fusion partner gene of MLL, in a therapy-related acute myeloid leukemia with a t(11;17)(q23;q25). *Proc. Natl. Acad. Sci. USA*. 96:6428–6433. http://dx.doi.org/10.1073/pnas.96.11.6428

Pedersen, S.F., J.W. Mills, and E.K. Hoffmann. 1999. Role of the F-actin cytoskeleton in the RVD and RVI processes in Ehrlich ascites tumor cells. *Exp. Cell Res.* 252:63–74. http://dx.doi.org/10.1006/excr.1999.4615

Renkawitz, J., and M. Sixt. 2010. Mechanisms of force generation and force transmission during interstitial leukocyte migration. *EMBO Rep.* 11:744–750. http://dx.doi.org/10.1038/embor.2010.147

Riedl, J., A.H. Crevenna, K. Kessenbrock, J.H. Yu, D. Neukirchen, M. Bista, F. Bradke, D. Jenne, T.A. Holak, Z. Werb, et al. 2008. Lifeact: A versatile marker to visualize F-actin. *Nat. Methods*. 5:605–607. http://dx.doi.org/10.1038/nmeth.1220

Rodal, A.A., L. Kozubowski, B.L. Goode, D.G. Drubin, and J.H. Hartwig. 2005. Actin and septin ultrastructures at the budding yeast cell cortex. *Mol. Biol. Cell*. 16:372–384. http://dx.doi.org/10.1091/mbc.E04-08-0734

Sahai, E., and C.J. Marshall. 2003. Differing modes of tumour cell invasion have distinct requirements for Rho/ROCK signalling and extracellular proteolysis. *Nat. Cell Biol.* 5:711–719. http://dx.doi.org/10.1038/ncb1019

Shankar, J., A. Messenberg, J. Chan, T.M. Underhill, L.J. Foster, and I.R. Nabi. 2010. Pseudopodial actin dynamics control epithelial-mesenchymal transition in metastatic cancer cells. *Cancer Res.* 70:3780–3790. http://dx.doi.org/10.1158/0008-5472.CAN-09-4439

Sheetz, M.P. 2001. Cell control by membrane-cytoskeleton adhesion. *Nat. Rev. Mol. Cell Biol.* 2:392–396. http://dx.doi.org/10.1038/35073095

Speare, J.O., D.K. Offerdahl, A. Hasenkrug, A.B. Carmody, and G.S. Baron. 2010. GPI anchoring facilitates propagation and spread of misfolded Sup35 aggregates in mammalian cells. *EMBO J.* 29:782–794. http://dx.doi.org/10.1038/emboj.2009.392

Spiliotis, E.T., M. Kinoshita, and W.J. Nelson. 2005. A mitotic septin scaffold required for Mammalian chromosome congression and segregation. *Science*. 307:1781–1785. http://dx.doi.org/10.1126/science.1106823

Stewart, M.P., J. Helenius, Y. Toyoda, S.P. Ramanathan, D.J. Muller, and A.A. Hyman. 2011. Hydrostatic pressure and the actomyosin cortex drive mitotic cell rounding. *Nature*. 469:226–230. http://dx.doi.org/10.1038/nature09642

Stock, C., and A. Schwab. 2006. Role of the Na/H exchanger NHE1 in cell migration. *Acta Physiol. (Oxf.)*. 187:149–157. http://dx.doi.org/10.1111/j.1748-1716.2006.01543.x

Surka, M.C., C.W. Tsang, and W.S. Trimble. 2002. The mammalian septin MSF localizes with microtubules and is required for completion of cytokinesis. *Mol. Biol. Cell*. 13:3532–3545. http://dx.doi.org/10.1091/mbc.E02-01-0042

Tada, T., A. Simonetta, M. Batterton, M. Kinoshita, D. Edbauer, and M. Sheng. 2007. Role of Septin cytoskeleton in spine morphogenesis and dendrite development in neurons. *Curr. Biol.* 17:1752–1758. http://dx.doi.org/10.1016/j.cub.2007.09.039

Tamma, G., G. Procino, M. Svelto, and G. Valenti. 2007. Hypotonicity causes actin reorganization and recruitment of the actin-binding ERM protein moesin in membrane protrusions in collecting duct principal cells. *Am. J. Physiol. Cell Physiol.* 292:C1476–C1484. http://dx.doi.org/10.1152/ajpcell.00375.2006

Tanaka-Takiguchi, Y., M. Kinoshita, and K. Takiguchi. 2009. Septin-mediated uniform bracing of phospholipid membranes. *Curr. Biol.* 19:140–145. http://dx.doi.org/10.1016/j.cub.2008.12.030

Tooley, A.J., J. Gilden, J. Jacobelli, P. Beemiller, W.S. Trimble, M. Kinoshita, and M.F. Krummel. 2009. Amoeboid T lymphocytes require the septin cytoskeleton for cortical integrity and persistent motility. *Nat. Cell Biol.* 11:17–26. http://dx.doi.org/10.1038/ncb1808

Xie, Y., J.P. Vessey, A. Konecna, R. Dahm, P. Macchi, and M.A. Kiebler. 2007. The GTP-binding protein Septin 7 is critical for dendrite branching and dendritic-spine morphology. *Curr. Biol.* 17:1746–1751. http://dx.doi.org/10.1016/j.cub.2007.08.042